

## Radii of Rydberg states of isolated silicon donors

**Citation for published version:**

Li, J, Nguyen, HL, Litvinenko, KL, Clowes, SK, Engelkamp, H, Pavlov, SG, Hübers, H-W, Shuman, VB, Portsel, LM, Lodykin, AN, Astrov, YA, Abrosimov, NV, Pidgeon, CR, Fisher, A, Zeng, Z, Niquet, Y-M & Murdin, BN 2018, 'Radii of Rydberg states of isolated silicon donors', *Physical Review B*, vol. 98, no. 8, 085423. <https://doi.org/10.1103/PhysRevB.98.085423>

**Digital Object Identifier (DOI):**

[10.1103/PhysRevB.98.085423](https://doi.org/10.1103/PhysRevB.98.085423)

**Link:**

[Link to publication record in Heriot-Watt Research Portal](#)

**Document Version:**

Peer reviewed version

**Published In:**

Physical Review B

**Publisher Rights Statement:**

©2018 American Physical Society. This is the accepted version of a paper accepted for publication in Physical Review B.

**General rights**

Copyright for the publications made accessible via Heriot-Watt Research Portal is retained by the author(s) and / or other copyright owners and it is a condition of accessing these publications that users recognise and abide by the legal requirements associated with these rights.

**Take down policy**

Heriot-Watt University has made every reasonable effort to ensure that the content in Heriot-Watt Research Portal complies with UK legislation. If you believe that the public display of this file breaches copyright please contact [open.access@hw.ac.uk](mailto:open.access@hw.ac.uk) providing details, and we will remove access to the work immediately and investigate your claim.

# Radii of Rydberg States of Isolated Silicon Donors

Juerong Li<sup>1</sup>, Nguyen H. Le<sup>1</sup>, K. Litvinenko<sup>1</sup>, S.K. Clowes<sup>1</sup>, H. Engelkamp<sup>2</sup>, S.G. Pavlov<sup>3</sup>, H.-W. Hübers<sup>3,4</sup>, V.B. Shuman<sup>5</sup>, L.M. Portsel<sup>5</sup>, A.N. Lodygin<sup>5</sup>, Yu.A. Astrov<sup>5</sup>, N.V. Abrosimov<sup>6</sup>, C.R. Pidgeon<sup>7</sup>, A. Fisher<sup>8</sup>, Zaiping Zeng<sup>9</sup>, Y-M Niquet<sup>9</sup>, B.N. Murdin<sup>1</sup>

<sup>1</sup>*Advanced Technology Institute, University of Surrey, Guildford, GU2 7XH, UK*

<sup>2</sup>*High Field Magnet Laboratory (HFML-EMFL), Radboud University, Toernooiveld 7, 6525 ED Nijmegen, The Netherlands*

<sup>3</sup>*Institute of Optical Sensor Systems, German Aerospace Center (DLR), Rutherfordstr. 2, 12489 Berlin, Germany*

<sup>4</sup>*Humboldt Universität zu Berlin, Institut für Physik, Newtonstr. 15, 12489 Berlin, Germany*

<sup>5</sup>*Ioffe Institute, Russian Academy of Sciences, St. Petersburg, Russia*

<sup>6</sup>*Leibniz Institute for Crystal Growth, Berlin, Germany*

<sup>7</sup>*Institute of Physics and Quantum Science, SUPA, Heriot-Watt University, Edinburgh, EH14 4AS*

<sup>8</sup>*London Centre for Nanotechnology and Department of Physics and Astronomy, University College London, London WC1H 0AH, UK*

<sup>9</sup>*Université Grenoble Alpes, CEA, INAC-MEM, L\_Sim 38000 Grenoble, France*

## Abstract

**We have performed a high field magneto-absorption spectroscopy on silicon doped with a variety of single and double donor species. The magnetic field provides access to an experimental magnetic length, and the quadratic Zeeman effect in particular may be used to extract the wavefunction radius without reliance on previously determined effective**

mass parameters. We were therefore able to determine the limits of validity for the standard one-band anisotropic effective mass model. We also provide improved parameters and use them for an independent check on the accuracy of effective mass theory. Finally, we show that the optically accessible excited state wavefunctions have the attractive property that interactions with neighbours are far more forgiving of position errors than (say) the ground state.

## **Introduction**

Impurities in silicon provide a platform for classical microelectronics and quantum technology. Knowledge of the wavefunction extent is needed for prediction of the interaction between donors and their neighbours for tests of physics<sup>[1][2][3][4]</sup>, device transport<sup>[5]</sup> and entanglement/gating<sup>[6][7][8][9]</sup>. With knowledge of the extent the atoms may be appropriately placed to optimize these interactions<sup>[10][11]</sup>. Qubit schemes being currently investigated that use excited states include a variety of species <sup>[6][12]</sup> including double donors like selenium<sup>[13]</sup>. Amazingly, in spite of their ubiquity and enormous technical importance, there is no measurement of the state radius of any isolated silicon impurity after more than six decades of research<sup>[14]</sup>. Regular arrays are desired for quantum computer architectures<sup>[7][8][9]</sup>, for which information on the neighbour-neighbour interactions will be crucial - just as it is for free atoms<sup>[15]</sup>. Because wavefunctions decay exponentially, a rapid change in the coupling occurs as a function donor-donor separation<sup>[4]</sup> – this is the single impurity equivalent of the Mott metal-insulator transition – control of the coupling requires good information on the separation at which the change occurs. Indeed the simplest experimental way to access the wavefunction extent is via the metal-insulator transition for ground states and a similar transition occurs for excited states<sup>[16]</sup>, however this is a complicated many-body problem and its precise details are unclear, so that it can only be used approximately for the ground state of single donors, not at all for double donors (because they produce half-full and full impurity bands respectively). Without knowledge of the wavefunction extent we cannot engineer the contact of the impurity

with readout electronics<sup>[5]</sup> external leads (source, drain, gates etc) or to know how much control is required to construct a dimer<sup>[4]</sup>, a chain<sup>[6]</sup> or a lattice<sup>[3]</sup>. The questions we raise here are closely analogous to those for cold Rydberg atoms in magnetic traps, where the excited states are large and highly susceptible to magnetic fields (as in our case), and so are the dipole moments and interactions with neighbouring atoms which affects both the spectra<sup>[17]</sup> and the formation of condensates<sup>[18]</sup>, though in this case the ion is fixed, and we have the extra complication of an anisotropic effective mass.

Here we show that the wavefunction radius for excited states can be found directly from the ratio of the coefficients of the linear and quadratic Zeeman effects (LZE and QZE) without the need for any effective mass parameters, and provide the first radius measurement of hydrogenic impurity excited states. Effective Mass Theory (EMT)<sup>[14][19][20][21][23]</sup> may be used to predict the spectrum and the wavefunction radius from three parameters; two effective mass values and the permittivity. We provide a self-consistent set of parameters obtained only from the zero-field spectrum and LZE, and use the resulting prediction for the QZE as an independent check on the validity of EMT.

There are currently two primary methods to detect wavefunction properties experimentally: via electron spin resonance (ESR) which measures contact with the donor nucleus; or via tunnelling methods which measure contact with the surface/barrier nearby. ESR<sup>[24][25][26]</sup> is excellent for determining the central part of the wavefunction but not necessarily the long range part that would be responsible for coupling to neighbours. Recently images of the ground state wavefunction of near-surface impurities have been obtained from Scanning Tunneling Microscopy (STM)<sup>[27][28][29][30]</sup> which allows direct observation of the density where the donor wavefunctions touch the surface. The images are complicated to interpret with high accuracy because the signal due to the donor is a small modulation on top of the density due to the surface atoms, and a very careful Fourier Transform filtering and other processing is

required<sup>[28]</sup>. Tunneling spectroscopy of donors in contact with a barrier is also possible<sup>[31][32]</sup>. In either case, imaging and tunnelling spectroscopy are limited to near-interface states that are naturally strongly perturbed. ESR and tunneling spectroscopy have only been used to extract the state radius for the ground state. Extraction of ground state dimensions from the QZE is also possible, but more assumptions are required<sup>[33][34]</sup>.

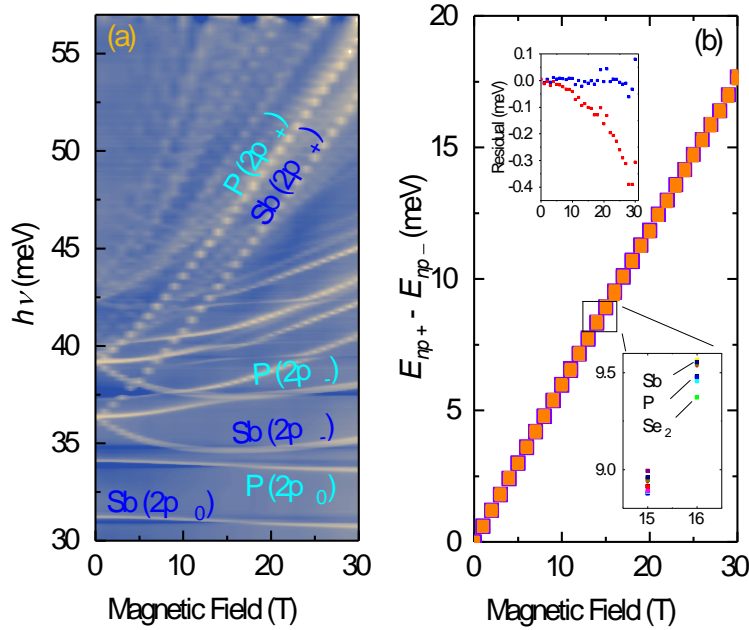


**Fig. 1** Linear Zeeman effect. a) Lyman series of the Si:P,Sb co-doped sample. Labels indicate the excited state for three of the strongest Lyman series transitions. The colour scale indicates the transmission (dark blue =high transmission; light yellow = high absorption). b) Splitting between the transitions for same  $n$  but different  $m$ , i.e.  $h\nu_{1s \rightarrow np+} - h\nu_{1s \rightarrow np-} = E_{np+} - E_{np-}$  against  $B$ . Data presented are for  $n=2$  and 3 for all species used in this work (Si:X where X=Li,P,Sb,Bi,Mg,Se,Se<sub>2</sub>,S) showing they all follow the same field dependence. Inset bottom: Expanded scale section from main panel showing sixteen points at each field with a different colour symbol for each species/ $n$  combination (and only three examples are labelled due to the small scatter). Inset top: residuals from the linear fit (red) and from the non-parabolic model fit (blue) to the Si:P data from the main panel.

## Experiment

In this work we investigate the excited state wavefunction extent from the magnetic length. We investigated the QZE in bulk doped silicon with single substitutional donors Bi, Sb or P<sup>[35][36]</sup>, the single interstitial donor Li, substitutional double donors S<sup>[38][39]</sup>, Se<sup>[33][40]</sup>, the interstitial double donor Mg<sup>[41]</sup>, and double donor complexes S<sub>2</sub> and Se<sub>2</sub>. The doping of each was in the range  $1 \times 10^{14}$  to  $2 \times 10^{15} \text{ cm}^{-3}$ , low enough that the distance between the donors is far larger than the orbit radius of any of the states of interest. We performed infrared transmission spectroscopy at  $T=1.4\text{K}$  as a function of magnetic field up to  $B=30\text{T}$ , in the Faraday configuration. All the samples were cut into [001] wafers and bevelled to  $1^\circ$  to avoid Fabry-Perot interference, and the resolution was  $0.04 \text{ meV}$  determined by residual water vapour absorption lines. Data for the Si:P and Si:Li samples were resolution limited. The transmitted intensity was recorded as a function of frequency and field,  $I(\nu, B)$ . The median of  $I(\nu, B)$  across all magnetic fields at each frequency was used to find the field-independent background spectrum,  $I_{\text{background}}(\nu)$ , and hence the transmission  $T(\nu, B) = I(\nu, B) / I_{\text{background}}(\nu)$ , as in the example of Fig 1a (see [35] for more experimental details). The transmission spectrum shows well resolved absorption lines and clear evidence of the LZE (e.g. in the splitting of the  $2p_+$  and  $2p_-$  transitions at low field) and the QZE (e.g. in the curvature of the  $2p_-$  at high field).

## Perturbation theory for excited states

Effective mass theory (EMT)<sup>[14][19][20][21][22][23]</sup> predicts hydrogenic donor states very well using length, energy and field parameters  $a_B^* = a_B \epsilon_r / m_t^*$ ,  $E_H^* = E_H m_t^* / \epsilon_r^2$  and  $B_a^* = \hbar / e a_B^{*2} = \hbar m_t^{*2} / e a_B^2 \epsilon_r^2$  that are scaled from the atomic hydrogen Bohr radius, Hartree energy and atomic unit of magnetic field respectively by the relative effective mass  $m_t^*$  and relative dielectric constant  $\epsilon_r$ . Silicon is indirect and the conduction band minimum is far from  $k=0$  near the six equivalent X-points of the Brillouin zone (along the  $\langle 001 \rangle$  directions). These six valleys are anisotropic, characterized by a mass transverse to the valley axis  $m_t^*$  and a mass anisotropy parameter,  $\gamma (=m_t^* / m_l^*$  where  $m_l^*$  is the mass along the axis). According to the Kohn-

Luttinger<sup>[19]</sup> EMT model, inter-valley interactions are to be ignored (or treated later by perturbation theory), and the single valley wavefunction is taken to be the product of a slowly varying envelope and quickly varying terms:  $\psi_{j,\mu}(\mathbf{r}) = f_{j,\mu}(\mathbf{r})e^{i\mathbf{k}_\mu \cdot \mathbf{r}}$  where  $\mathbf{k}_\mu$  is the momentum at the bottom of the valley with index  $\mu$  (i.e.  $\mathbf{k}_\mu$  is along  $x$ ,  $-x$ ,  $y$ ,  $-y$ ,  $z$ ,  $-z$  and  $|\mathbf{k}_\mu| = 0.85\pi/a = k_0$  where  $a$  is the lattice constant) and  $j$  is an index (or set of indices) identifying which state within the valley. Using single-valley EMT works well for the excited state energies<sup>[14]</sup> (and our aim here is to assess the accuracy of the radius prediction for the excited states). We ignored an additional lattice-periodic factor<sup>[19][22][23]</sup> since it does not influence any of what follows or the intended application of engineering donor-donor interactions. The envelope functions  $f_{j,\mu}$  are solutions of  $\hat{H}_\mu f_{j,\mu} = \varepsilon_j f_{j,\mu}$ . In the case that a magnetic field is applied parallel to the axis of the  $z$ -valley, the Hamiltonian for that valley is<sup>[14][33][34][35][36]</sup>

$$\hat{H}_z = -\frac{E_H^* a_B^{*2}}{2} \left[ \frac{\partial^2}{\partial x^2} + \frac{\partial^2}{\partial y^2} + \gamma \frac{\partial^2}{\partial z^2} \right] - \frac{E_H^* a_B^*}{r} + \frac{E_H^* B L_z}{2 B_a^* \hbar} + \frac{E_H^* B^2 (x^2 + y^2)}{8 B_a^{*2} a_B^{*2}} \quad (1)$$

The first two terms comprise the zero-field Hamiltonian for hydrogen including the mass anisotropy,  $\hat{H}_{0z}$ . We neglect tetrahedral corrections to the impurity potential<sup>[37]</sup>. The last two are respectively the LZE and QZE terms  $\hat{H}_1$  and  $\hat{H}_2$ . For other valleys and field directions the Hamiltonian is more complex and we shall not concern ourselves with such cases. Comparison of the eigenvalues of Eqn (1) with the experimental zero field energy spectrum allows extraction/verification of  $E_H^*$  and  $\gamma$  only, and the LZE allows extraction of  $B_a^*$ . If it is assumed Eqn (1) holds, and therefore  $B_a^* = \hbar/ea_B^{*2}$ , this is enough to predict  $a_B^*$ . In this work we measure the ratio of the QZE and LZE, which is a means to extract the radius directly, and provides in essence experimental measurement of  $B_a^* a_B^{*2}$  as a test of the validity of Eqn (1). In other words, whereas the zero-field spectrum and LZE can provide tests of the scaling rules given at the beginning of the paragraph for  $E_H^*$  and  $B_a^*$ , only the QZE can test the scaling rule for  $a_B^*$  independently.

Eqn (1) has cylindrical symmetry about  $z$  so the azimuthal dependence of the wavefunction envelope is  $e^{im\phi}$ , which is an eigenfunction of the LZE term with quantum number  $m$ , the

magnetic quantum number. For our field direction ( $\mathbf{B}/z$ )  $\hat{H}_1$  commutes with  $\hat{H}_{0z}$  and  $\hat{H}_2$  so there are no off-diagonal matrix elements of  $\hat{H}_1$ , and the magnetic quantum number,  $m$ , is conserved for all  $B$ . The LZE energy  $E_1 = \mu_B^* m B$  is therefore well defined for all  $B$ .  $\hat{H}_{0z}$  and  $\hat{H}_2$  do not commute, but for sufficiently small field we can treat  $\hat{H}_2$  by perturbation theory which produces

$$E(B) = E_0 + \mu_B^* m B + \frac{e\mu_B^*}{4\hbar} \rho_0^2 B^2 \quad (2)$$

where  $\rho_0$  is the value of the transverse radius  $\rho = \sqrt{\langle x^2 + y^2 \rangle}$  at zero field. The effective Bohr magneton  $\mu_B^* = E_H^*/2B_a^* = eE_H^* a_B^{*2}/2\hbar = \mu_B/m_t^*$ , and we substituted  $E_H^*/B_a^{*2} a_B^{*2} = 2e\mu_B^*/\hbar$ . As we shall see,  $E(B)$  becomes non-parabolic at high field because  $\rho$  shrinks due to magnetic confinement so that the small perturbation approximation fails (when  $E_2 = e\mu_B^* \rho_0^2 B^2/4\hbar$  becomes significant compared with  $E_0$ ). In this case  $\hat{H}_{0z}$  and  $\hat{H}_2$  are mixed and their contributions cannot be separated. We define an effective transverse radius,  $\tilde{\rho}$ , given by

$$\frac{d^2 E}{dB^2} = \frac{e\mu_B^*}{2\hbar} \tilde{\rho}^2 \quad (3)$$

which is equal to the actual transverse radius at low field i.e.  $\tilde{\rho}^2(0) = \rho_0^2$  as shown by Eqn (2). It is useful to note that  $\hat{H}_{0z}$  and  $\hat{H}_2$  have the same symmetry for  $\mathbf{B}/z$ , so solving eigenvalues and eigenfunctions of Eqn (1) for  $B \neq 0$  is no more difficult than for  $B=0$ . For other field directions  $\hat{H}_{0z}$ ,  $\hat{H}_1$  and  $\hat{H}_2$  are all mutually non-commuting and  $m$  is not a good quantum number.

### **Linear Zeeman effect**

We require the ratio of the QZE and LZE terms in Eqn (2), and we start with the LZE. It is easy to extract  $\mu_B^*$  directly from the experimental field dependence for  $\mathbf{B}/z$  because the linear Zeeman energy is well defined and  $m$  is a good quantum number: we simply take the difference between the transition energies to the  $np_+$  and  $np_-$  excited states:  $h\nu_{1s \rightarrow np_+} - h\nu_{1s \rightarrow np_-} = E_{np_+} - E_{np_-} = 2\mu_B^* B$ . Since  $\hat{H}_1$  commutes with  $\hat{H}_{0z}$  and  $\hat{H}_2$ , the quadratic and zero-field terms cancel exactly. It can be seen from Fig 1b that this linear relationship holds very well, and the slope  $2\mu_B^* = 2\mu_B/m_t^*$  holds for all species and for both  $2p_{\pm}$  and  $3p_{\pm}$  excited states. At the



highest fields used, there is a slight departure from linearity – the slope decreases at higher energy (Fig 1b inset shows the residuals) which must have resulted from an effective mass increase. We presume that the mass increase arises due to the higher frequency Fourier components in the envelope-function introduced by the constriction with field, and therefore the increase is equal for both  $p_+$  and  $p_-$  states with the same  $n$ . If the mass rises with field and is an even function, a suitable non-parabolicity correction to the form of Fig 1b is  $E_{np+} - E_{np-} = 2\mu_B^* B / (1 + B^2/B_{np}^2)$  and a fit to the Si:P  $2p_{\pm}$  data gives the values of  $\mu_B^*$  and  $B_{np}$  in Table 1, which also shows the inferred value of  $m_t^*$ .

Fit parameters	Value
$\mu_B^*$	$0.2978 \pm 0.0003 \text{ meV/T}$
$B_{np}$	$242 \pm 12 \text{ T}$
$\gamma$	$0.2096 \pm 0.0002$
$E_H^*$	$39.83 \pm 0.03 \text{ meV}$
Inferred parameters	Value
$m_t^*$	$0.1944 \pm 0.0002$
$m_l^*$	$0.927 \pm 0.001$
$\epsilon_r$	$11.52 \pm 0.01$
$a_B^*$	$3.137 \pm 0.004 \text{ nm}$
$B_a^*$	$66.88 \pm 0.09 \text{ T}$

**Table 1.** Effective mass parameters obtained.

Our value of  $m_t^*$  is  $2.0 \pm 0.1\%$  larger than the band edge value,  $0.1905 \pm 0.0001$  from cyclotron resonance for free electrons<sup>[20]</sup> and closer to that derived from the approach of Fig 1b by others ( $0.195 \pm 0.002$ <sup>[42]</sup>), though with higher precision here; this is also presumably due to the non-parabolicity, since the appropriate value for a donor is an average over a region of  $k$ -space around the c.b. minimum, the extent of which is given by the reciprocal of the wavefunction and evidently includes enough to noticeably increase  $m_t^*$ . Applying the same fit procedure to the Si:P  $3p_{\pm}$  data produces a value of  $\mu_B^*$  that is  $1.3 \pm 0.1\%$  larger than the band edge value, i.e. the difference is less than for  $2p_{\pm}$  as would be expected for a state that is larger in real space and smaller in reciprocal space.

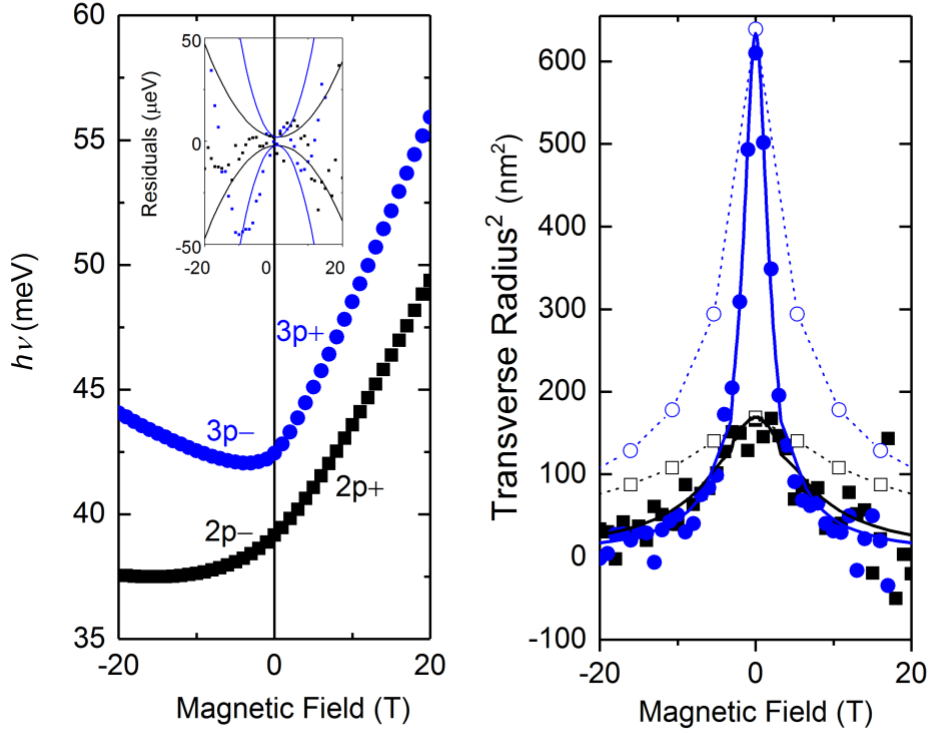


**Fig. 2** Quadratic Zeeman effect. a) Transition energy,  $h\nu_{1s \rightarrow np\pm}$ , for Si:P for  $2p\pm$  (squares) and  $3p\pm$  (circles), with  $m=+1$  transitions shown at positive field and  $m=-1$  transitions shown at negative field. The fits described in the text produced the residuals shown as an inset, along with the weighting function used. b) The transverse radius. The effective transverse radius squared for the transition, i.e.  $\tilde{\rho}_{np\pm}^2 - \tilde{\rho}_{1s}^2$  found by applying Eqn (3) to the experimental  $h\nu_{1s \rightarrow np\pm}(B)$  shown in (a), (filled symbols) using the Savitzky-Golay method. Also shown is the theoretical effective transverse radius, i.e. Eqn (3) applied to  $E_{np\pm}(B)$  from EMT with the parameters from Table 1 (not a fit), solid lines. The open symbols show,  $\rho^2$ , the actual (as opposed to effective) transverse radius squared  $\langle x^2 + y^2 \rangle$  of the excited states from the EMT wavefunctions (with the same parameters, not a fit). The effective radius,  $\tilde{\rho}$ , and actual radius,  $\rho$ , are clearly the same at small field.

### Quadratic Zeeman effect

It is also easy to extract the transverse radius directly from the experiment. The second derivative of the transition energy is, from Eqn (3),  $\frac{2\hbar}{e\mu_B^*} \frac{d^2}{dB^2} h\nu_{1s \rightarrow np\pm} = \frac{2\hbar}{e\mu_B^*} \frac{d^2}{dB^2} [E_{np\pm} - E_{1s}] = \tilde{\rho}_{np\pm}^2 - \tilde{\rho}_{1s}^2$ . Since  $\hat{H}_1$  commutes with  $\hat{H}_{0z}$  and  $\hat{H}_2$ , the radius and its constriction with

field do not depend on  $m$ , and hence the transverse radius at zero field  $\rho_{np-}^2(0) = \rho_{np+}^2(0)$ . Therefore, in order to extract the double derivative at  $B=0$  more accurately we may plot the transition energy vs field for  $1s \rightarrow np_+$  and  $1s \rightarrow np_-$  back to back (Fig 2a). The experimental results for  $\tilde{\rho}_{np\pm}^2 - \tilde{\rho}_{1s}^2$  for Si:P is shown in Fig 2b. Although we can see approximately the zero-field value from the figure, data extracted from derivatives of experimental data are always noisy, and it is preferably to extract the radius from fitting the raw data. We therefore need an analytical approximation for the QZE. Noting that the experimental dependence on Fig 2b resembles a Lorentzian with zero-field value  $\rho_0^2$ , i.e.  $\tilde{\rho}^2 \approx \rho_0^2(1 + B^2/B_c^2)^{-1}$ , where  $B_c$  is a parameter describing the field scale at which the constriction occurs, a suitable form is  $E_2(B) = \frac{e\mu_B^*}{2\hbar}\rho_0^2 B_c^2 g(B/B_c)$  where  $g(x) = x \arctan(x) - \frac{1}{2}\ln(x^2 + 1)$  (the double derivative of which produces the desired Lorentzian). We therefore performed a fit of

$$E(B) = E_0 + \frac{\mu_B^*}{1 + B^2/B_{np}^2} \left[ B + \frac{e}{2\hbar} \rho_0^2 B_c^2 g\left(\frac{B}{B_c}\right) \right] \quad (4)$$

with free parameters  $\rho_0$ ,  $E_0$  and  $B_c$  (and fixed  $B_{np}$ ,  $\mu_B^*$  determined above). Crucially the factor  $e\rho_0^2/2\hbar$ , i.e. the ratio of the coefficients of the linear term and the QZE, does not depend on any effective mass parameters. The fit was weighted towards the data around  $B=0$  (since this is where  $\rho^2 = \tilde{\rho}^2$ ) with a quadratic weighting function shown in the inset of Fig 2a along with the residuals. We obtained values for the zero field radius of  $\rho_{2p\pm}^2 - \rho_{1s}^2 = 159 \pm 1 \text{ nm}^2$  and  $\rho_{3p\pm}^2 - \rho_{1s}^2 = 611 \pm 5 \text{ nm}^2$ , and the corresponding values of  $E_0$ , the zero-field transition energy, were  $39.161 \pm 0.001 \text{ meV}$  and  $42.453 \pm 0.001 \text{ meV}$  respectively.

### **Separating the ground state contribution to the transition QZE**

For hydrogen we expect  $\rho_{1s}^2/\rho_{np\pm}^2 = n^{-4}$  and in Si:P the 1s radius is further reduced by the central cell correction (CCC) – a short range potential that includes changes to the coulomb potential where the electron penetrates into the ion core and increases the binding energy, so  $\rho_{1s}^2$  contributes negligibly to the QZE of the  $1s \rightarrow np_{\pm}$  transition. In this approximation  $\rho_{2p\pm} = 12.61 \pm 0.03 \text{ nm}$  and  $\rho_{3p\pm} = 24.7 \pm 0.1 \text{ nm}$ . The ratio of these values is not exactly 4/9 simply because of the effect of mass anisotropy. Note that so far we have not used any EMT

calculations or any assumed effective mass parameters, we only took the form of Eqn (2) to be correct.

The effective mass approximation is not expected to hold for the ground state, which is small, and also subject to the CCC. The precise functional form of the CCC is unknown; only its symmetry and the end effect on the energy of the ground state are known. EMT is therefore untrustworthy for the ground state. The CCC mixes the six valley 1s states, and the resulting lowest energy component is the one labelled 1s(A<sub>1</sub>) (except in the case of Si:Li). Because this mixing introduces valleys transverse to the field for which Eqns 1 & 2 do not hold,  $\tilde{\rho}_{1s(A_1)}(0)$  is not simply related to the actual zero field transverse radius  $\rho_{1s(A_1)}$ . We performed Tight Binding calculations<sup>[43]</sup> in the range 0-30T, and extracted values of radius, and of the effective transverse radius by fitting a quadratic to  $E_{1s(A_1)}(B)$ , as shown in Table 2. The calculations were done with the  $sp^3d^5s^*$  model<sup>[44]</sup>, in supercells with side  $L = 48a = 26$  nm. On-site corrections were included on the impurity atom<sup>[45]</sup>. We can see that  $\tilde{\rho}_{1s(A_1)}^2(0)$  is about 1% of  $\rho_{np\pm}^2 - \tilde{\rho}_{1s(A_1)}^2(0)$  or less (note we abbreviated  $\tilde{\rho}_{1s(A_1)}^2$  to  $\rho_{1s}^2$  at the end of the previous section), and this confirms that it may be neglected for the purpose of studying the excited states.

	$r_{1s(A_1)}$ (nm)	$\rho_{1s(A_1)}$ (nm)	$\frac{e\mu_B^*}{4\hbar} \tilde{\rho}_{1s(A_1)}^2$ (neV/T <sup>2</sup> )	$\tilde{\rho}_{1s(A_1)}^2$ (nm <sup>2</sup> )
P	2.481	2.026	255	2.240
As	2.125	1.735	181	1.590
Sb	2.608	2.130	284	2.495
Bi	1.630	1.331	99	0.870

**Table 2.** Tight Binding results. The zero-field 3D radius  $r_{1s(A_1)} = \sqrt{3\langle z^2 \rangle}$  (and the 2D radius  $\rho_{1s(A_1)} = \sqrt{\frac{2}{3}}r_{1s(A_1)}$ ) were calculated from the TB wavefunctions. The QZE field tuning constant was found by calculating the binding energy from 0-30T and fitting with a quadratic. For the conversion to  $\tilde{\rho}_{A_1}^2$ , we used the value of  $\mu_B^*$  in Table 1.

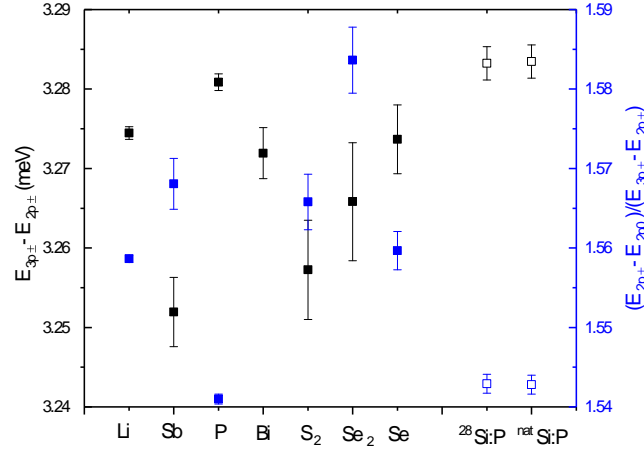


**Figure 3.** Experimentally determined values of the zero-field energy splittings between excited states for different donor centres in silicon. Centres are displayed in order of binding energy. Data from Ref [46] are also included as open symbols. Error bars are from Gaussian fits (this work, or in the case of [46] the instrumental resolution).

### Exact diagonalization of single valley QZE

We also investigated the detailed predictions of EMT by finding the eigen-values and eigen-functions of Eqn (1). Three independent parameters are required in Eqn (1) are:  $E_H^*$ ,  $a_B^*$  and  $\gamma$  (recall that  $B_a^* = \hbar/ea_B^{*2}$ ), which may be found from  $\epsilon_r, m_t^*$  and  $\gamma$  or vice-versa. We follow the procedure of Faulkner<sup>[21]</sup> to extract  $E_H^*$  (which determines the energy scale) and  $\gamma$  (which determines the fractional splitting between the  $p_0$  and  $p_{\pm}$  states) by comparison of the zero field energy spectrum with the eigenvalues of  $\hat{H}_{0z}f_{j,z} = \epsilon_j f_{j,z}$  (i.e. in zero field), except that whereas Faulkner used a multivariate minimisation of variational solutions, we calculated  $f$  with a Lanczos method<sup>[35]</sup> (although our theoretical results for  $E_{npm}/E_H^*$  for different values of  $\gamma$  all agree extremely well with the earlier variational results). Faulkner noted that  $G = (E_{2p_{\pm}} - E_{2p_0})/(E_{3p_{\pm}} - E_{2p_{\pm}})$  depends only on  $\gamma$ . Taking the value of the ratio to be  $G=1.543 \pm 0.001$  appropriate for Si:P (Fig 3) gives the value of  $\gamma$  shown in Table 1. With this value the theoretical splitting  $E_{3p_{\pm}} - E_{2p_{\pm}} = 0.08243 E_H^*$  (and this is very insensitive to  $\gamma$ , it changes by only 0.1% over the range  $\gamma=0.18$  to 0.22). Taking the experimental  $E_{3p_{\pm}} - E_{2p_{\pm}} = 3.283 \pm 0.002$  meV

appropriate for Si:P (Fig 3) results in the value of  $E_H^*$  shown in Table 1. Faulkner's values of  $\gamma=0.2079$  and  $E_H^*=39.89\text{meV}$  (from  $G=1.555$  and  $E_{3p\pm} - E_{2p\pm}=3.28\text{meV}$ ) are very slightly different simply through use of better samples with sharper lines here. There is a very small variation among species ( $\sim 1\%$ ) in both experimental parameters on Fig 3 though the values for Si:P from the different experiments (this work and [46]) are remarkably consistent (differing by 0.05%). It is difficult to see a pattern in the values, and although the error bars are in some cases quite large compared with the variation, the case of Si:Li is notably different from Si:P within their respective error-bars (other species having larger error due to the broader, weaker lines), which is probably due the (very small but detectable) effects of the CCC on the excited states concerned.

Faulkner took  $m_t^*=0.1905$  (the band edge value from Hensel's earlier cyclotron resonance of free electrons<sup>[20]</sup>) and used his value of  $E_H^*$  to extract  $\epsilon_r$ . Using our result for  $m_t^*$  from the LZE from the same experiment (see above) is preferable for self-consistency, and results in the values of  $\epsilon_r, a_B^*$  etc shown in Table 1.

We calculated the eigenvalues of  $\hat{H}_{0z} + \hat{H}_1 + \hat{H}_2$  as a function of magnetic field along the valley axis with the Lanczos procedure. We extracted the transverse radius from the excited state wavefunctions: Fig 2b open symbols show  $\rho^2 = \langle x^2 + y^2 \rangle$  at a range of fields, and the zero-field values are given in Table 3. There are two ways to find the theoretical effective transverse radius  $\tilde{\rho}$  at zero field. Firstly we calculated the effective radius  $\tilde{\rho}^2(B)$  from the double derivative of the EMT results for  $E(B)$  using Eqn (3) (Fig 2b solid lines), and the zero-field value agrees very well with the zero-field value of the theoretical  $\rho$  (Fig 2b open symbols) as expected, which confirms the validity of Eqns (2) and (3). Then, to assess the procedure that was used to find the experimental  $\rho_0$  we performed a fit of Eqn (4) to the theoretical  $E(B)$ . In this case for the  $2p_{\pm}$  and  $3p_{\pm}$  we obtained  $\rho_0 = 4.08$  and  $7.86$  atomic units, i.e.  $12.8$  and  $24.7$  nm respectively. These values agree very well with the experimental values given earlier from

the fits of Eqn (4) to the experimental data, but are about 1% and 2% less, respectively, than the exact  $\rho_0$  obtained from the theoretical wavefunctions (Table 3). This discrepancy is too small to be visible on Fig 2b. It arises just because of the fact that our fitting process took the QZE radius constriction with field,  $\tilde{\rho}(B)$ , to be a Lorentzian function, which is an imperfect approximation. There may also be an additional systematic error in the experiment due to the fact we neglected the contribution of the ground state (which would raise the experimental results by about 1% and 0.2% respectively).

	$-E$ (meV)	$t$ (nm)	$l$ (nm)	$r$ (nm)	$\rho_0$ (nm)	$\gamma' (=l^2/t^2)$
1s	30.539	2.41	1.33	3.66	3.40	0.31
2p <sub>0</sub>	11.463	4.42	4.48	7.69	6.25	1.02
3p <sub>0</sub>	5.468	8.59	11.59	16.79	12.15	1.82
4p <sub>0</sub>	3.297	12.36	21.42	27.65	17.49	3.00
4f <sub>0</sub>	2.330	22.45	15.09	35.15	31.75	0.45
5p <sub>0</sub>	2.225	16.97	32.96	40.78	24.01	3.77
6p <sub>0</sub>	1.623	21.55	48.03	56.89	30.48	4.97
5f <sub>0</sub>	1.504	35.33	27.99	57.27	49.96	0.63
2p <sub>±</sub>	6.396	9.18	3.85	13.54	12.98	0.18
3p <sub>±</sub>	3.113	17.83	13.04	28.39	25.21	0.54
4p <sub>±</sub>	2.181	23.37	16.69	37.02	33.05	0.51
4f <sub>±</sub>	1.887	28.86	23.56	47.13	40.81	0.67
5p <sub>±</sub>	1.445	33.28	36.69	59.67	47.06	1.22
5f <sub>±</sub>	1.255	45.10	33.51	72.04	63.77	0.55
6p <sub>±</sub>	1.067	41.72	53.82	79.86	59.01	1.66

**Table 3.** Single valley state dimensions from EMT produced with the Lanczos method in zero field. The quantities listed are  $t = \sqrt{\langle x^2 \rangle} = \sqrt{\langle y^2 \rangle}$ ,  $l = \sqrt{\langle z^2 \rangle}$ ,  $r = \sqrt{2t^2 + l^2}$ ,  $\rho_0 = \sqrt{2}t$  and  $\gamma' = l^2/t^2$ . The effective mass parameters used were from Table 1. The 1s state mentioned is the single valley EMT state (ignoring the CCC).

## Discussion

We return to the motivation for this work, which was to examine the possibility for engineering overlap between neighbouring impurities for the purposes of quantum information applications. So far in this work we considered only the slowly varying envelope function, and

the need for obtaining high precision values for its radius. It is also important to remember that the wavefunction is modulated by quickly varying terms, and that these terms interfere for multi-valley wavefunctions<sup>[22][23]</sup>. Since valley interference is more commonly discussed in respect of the different components of the 1s ground state we illustrate the point with those states first. The single valley 1s states are mixed by the CCC and their degeneracy is lifted, and (apart from Si:Li) the ground state has  $A_1$  symmetry, meaning that the final wavefunction has the form  $\Psi_{1s(A_1)}(\mathbf{r}) = \frac{1}{\sqrt{6}} \sum_{\mu} \psi_{1s,\mu}(\mathbf{r}) = \frac{1}{\sqrt{6}} \sum_{\nu} \cos(k_0 x_{\nu}) f_{1s,\nu}(\mathbf{r})$  where  $\nu$  runs over  $x, y, z$ , i.e. there is a fast-oscillating, cosinusoidal term in each of the three dimensions. This state is therefore quickly oscillating in all three dimensions, as shown in Fig 4 (bottom left). Note that for the ease of illustration we put the lattice-periodic functions  $u(\mathbf{r}) = 1$  since it does not affect the general conclusions. Wavefunction plots for  $1s(A_1)$  with fewer approximations are available elsewhere<sup>[22][23]</sup>. The conduction band minima are 85% of the way from the  $\Gamma$  to the X-point, i.e.  $k_0 = 0.85\pi/a$  and so the  $\cos(k_0 x_{\nu})$  oscillation does not repeat with the lattice spacing. This means that there is a large change in wavefunction amplitude from atomic site to atomic site, which makes control over the overlaps difficult because they are extremely sensitive to position errors. We point out now that a significant advantage that can be obtained by using excited states to produce the coupling e.g. using the Stoneham-Fisher-Greenland scheme<sup>[6]</sup>. The advantage arises from the different valley interference. The high energy components of the ground state have E or  $T_2$  symmetry, and form a doublet and a triplet respectively. The three  $T_2$  states are quickly varying due to the valley interference in only one direction each: for example, one is  $\Psi_{1s(T_{2z})}(\mathbf{r}) = \sqrt{2} \sin(k_0 z) f_{1s,z}(\mathbf{r})$ , shown in Fig 4 (bottom middle). These  $T_2$  states are optically accessible from  $1s(A_1)$  for light polarised along  $z$ , although with much smaller oscillator strength than to the excited states with odd-parity envelopes such as the  $2p_-$  state. These  $T_2$  states would be very forgiving of position errors in two of the three dimensions ( $x$  and  $y$  in the case of the  $\Psi_{1s(T_{2z})}$  state illustrated). The E states oscillate with  $k_0$  in two dimensions ( $x, y$ ) and are therefore forgiving of positioning errors in the other dimension ( $z$ ). Returning to the odd-parity excited states of our experiment above, the



same advantage is obtained for the  $2p_-$  state in the  $z$ -valley,  $\Psi_{2p-(T_2z)}(\mathbf{r}) = \sqrt{2}\cos(k_0z)f_{2p-,z}(\mathbf{r})$ , which is also varying in only the  $z$ -direction (Fig 4 bottom right), and likewise the  $2p_+$  state. Note that the envelope  $f_{2p-,z}(r)$  is the same as the single valley EMT used earlier, since the CCC has no effect on excited states. It appears there is a strong motivation for utilizing the coupling between impurities mediated by THz pulses polarised in the plane, such as in schemes where the atoms in the ground  $1s(A_1)$  state are well isolated from each other, but during their excursion into the excited state they interact<sup>[6]</sup>. There may even be good reasons to investigate further donor species for which  $1s(E,T_2)$  is the ground state, such as Si:Li.

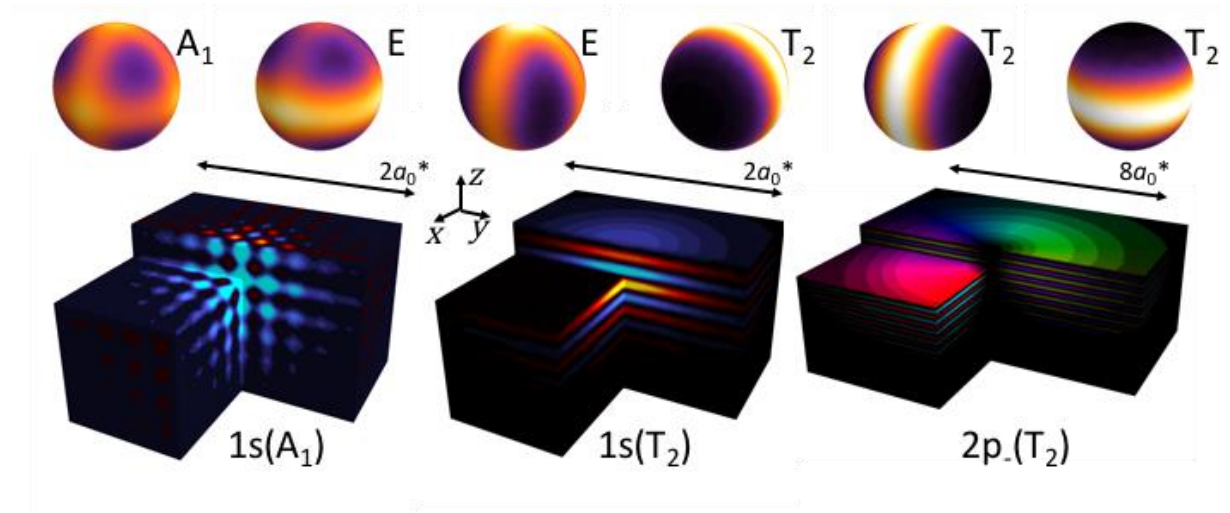


**Fig 4.** The wavefunctions. The top row shows the six ground state envelope functions: the colour scale shows the probability density increasing from black (zero density) to white, on a spherical surface around the donor averaged over a valley interference oscillation period. The bottom row shows some example wavefunctions including the valley interference term (but not the cell-periodic term). The brightness shows the probability density on some illustrative surfaces around the donor, and the colour scale shows the wavefunction phase. The donor is at  $\mathbf{r}=0$  at the central vertex of the image and the length scale is shown in units of  $a_0^*$ . The  $1s(T_2)$  state shown is the  $z$ -valley component (last one on the top row). All illustrations take the lattice periodic part of the wavefunction  $u(\mathbf{r}) = 1$  simplicity.

## **Conclusion**

In conclusion, we have measured the silicon donor excited state radii experimentally for the first time. We found an analytic form for the field dependence of the radius that fits the data very well, and agrees also with the results of a Lanczos solution to effective mass theory validating the EMT scaling rules. We showed that non-parabolicity effects become detectable above about 10T, and indeed that there is a detectable (0.7%) difference in the zero-field effective masses for the  $2p_{\pm}$  and  $3p_{\pm}$  states due to the higher frequency Fourier components in more tightly bound states the former. We provide high precision effective mass parameters for low (and zero) field. The excited state radii do not vary by more than 2% among a wide variety of species including double donors, and they provide a major advantages for donor-donor coupling due to the more favourable valley interference effects.

## **Acknowledgements**

We acknowledge financial support from the UK Engineering and Physical Sciences Research Council (COMPASSS/ADDRFSS, grant reference EP/H001905/1). The work at Nijmegen was performed as part of the research programme of the ‘Stichting voor Fundamenteel Onderzoek der Materie (FOM)’, which is financially supported by the ‘Nederlandse Organisatie voor Wetenschappelijk Onderzoek (NWO)’. Work on sample preparation is partially supported by the Russian Academy of Science according to program #8 "Physics of condensed matter and new materials". We would also like to thank Dr Ellis Bowyer for help with some of the experiments.

## **Data Availability**

The data from this work may be found at DOI: xxxxxx

## References

- [1] J.P. Dehollain et al, Bell's Inequality Violation with Spins in Silicon. *Nat Nano*, 2016. 11(3): p. 242-246.
- [2] J Salfi et al, Quantum simulation of the Hubbard model with dopant atoms in silicon, *Nat Commun*, 7, 11342, (2016) DOI: 10.1038/ncomms11342
- [3] Nguyen H. Le, Andrew J. Fisher, and Eran Ginossar, Extended Hubbard model for mesoscopic transport in donor arrays in silicon, *Phys. Rev. B* 96, 245406 (2017)
- [4] W. Wu et al, Excited states of defect linear arrays in silicon: A first-principles study based on hydrogen cluster analogs, *Phys. Rev. B* 97, 035205 (2018)
- [5] T Kobayashi et al, Resonant tunneling spectroscopy of valley eigenstates on a donor-quantum dot coupled system, *Appl Phys Lett*, 108, 152102 (2016) DOI: 10.1063/1.4945736
- [6] A. M. Stoneham, Fisher, A. J. & Greenland, P. T. Optically driven silicon-based quantum gates with potential for high-temperature operation. *J.Phys. Condens. Matter* 15, L447–L451 (2003).
- [7] CD Hill et al, A surface code quantum computer in silicon", *Science Advances* (2015) 1, e1500707, DOI: 10.1126/sciadv.1500707
- [8] G. Pica, B. W. Lovett, R. N. Bhatt, T. Schenkel, and S. A. Lyon, Surface code architecture for donors and dots in silicon with imprecise and nonuniform qubit couplings, *Phys. Rev. B* 93, 035306 (2016) DOI : 10.1103/PhysRevB.93.035306
- [9] G Tosi et al, Silicon quantum processor with robust long-distance qubit couplings, *Nature Communications* 8, 450 (2017)
- [10] SR Schofield et al. Atomically precise placement of single dopants in Si. *Phys. Rev. Lett.* 91, 136104 (2003).
- [11] SR Schofield et al, Quantum Engineering at the Silicon Surface Using Dangling Bonds. *Nature Communications*,. 4, 1649 (2013).
- [12] K. Saeedi et al, Optical Pumping and Readout of Bismuth Hyperfine States in Silicon for Atomic Clock Applications. *Scientific Reports*, 2015. 5: p. 10493.
- [13] K. J. Morse et al, A photonic platform for donor spin qubits in silicon, *Science Advances* 3, e1700930 (2017), DOI: 10.1126/sciadv.1700930
- [14] Pajot, B. Donor and donor-like EM spectra. in *Optical absorption of impurities and defects in semiconducting crystals: hydrogen-like centres*. (Springer, 2009)
- [15] S. Debnath, N. M. Linke, C. Figgatt, K. A. Landsman, K. Wright & C. Monroe "Demonstration of a small programmable quantum computer with atomic qubits", *Nature* 536, 63–66 (2016) doi:10.1038/nature18648
- [16] Thomas1981: G A Thomas, M Capizzi, F DeRosa, RN Bhatt, and TM Rice, *Phys. Rev.* 8 23, 5472, Appendix A (1981).
- [17] R. H. Garstang. Atoms in high magnetic-fields. *Prog. Phys.*, 40:105, 1977
- [18] T.Pohl, H.R.Sadeghpour, P.Schmelcher, "Cold and ultracold Rydberg atoms in strong magnetic fields" *Physics Reports* 484, 181 (2009) DOI: 10.1016/j.physrep.2009.10.001
- [19] W. Kohn and J. Luttinger, *Phys. Rev.* 98, 915 (1955). DOI 10.1103/PhysRev.98.915
- [20] J.C. Hensel, H. Hasegawa, and M. Nakayama, *Phys. Rev.* 138, A225 (1965)
- [21] Faulkner, RA, *Phys Rev B* 184, 713 (1969)
- [22] C. J. Wellard and L. C. L. Hollenberg Donor electron wave functions for phosphorus in silicon: Beyond effective-mass theory, *Phys Rev B* 72, 085202 (2005)
- [23] JK Gamble, NT Jacobson, E Nielsen, AD. Baczewski, JE. Moussa, I. Montano and RP Muller, Multivalley effective mass theory simulation of donors in silicon, *Physical Review B* 91, 235318 (2015)
- [24] G. Feher, *Phys. Rev.* 114, 1219 (1959)
- [25] E. B. Hale and R. L. Mieher, *Phys. Rev.* 184, 739 (1969)
- [26] G Pica, G Wolfowicz, M Urdampilleta, M L. W. Thewalt, H Riemann, N V. Abrosimov, P Becker, H-J Pohl, J J. L. Morton, R. N. Bhatt, S. A. Lyon, and B W. Lovett, Hyperfine Stark effect of shallow donors in silicon, *Phys. Rev. B* 90, 195204 (2014) DOI: 10.1103/PhysRevB.90.195204
- [27] K Sinthiptharakoon, SR Schofield, P Studer, V Brazdova, CF Hirjibehedin, DR Bowler and NJ Curson, Investigating individual arsenic dopant atoms in silicon using low-temperature scanning tunnelling microscopy *J. Phys.: Condens. Matter* 26 (2014) 012001 (8pp) doi:10.1088/0953-8984/26/1/012001
- [28] J. Salfi, J. A. Mol, R. Rahman, G. Klimeck, M. Y. Simmons, L. C. L. Hollenberg & S. Rogge, Spatially resolving valley quantum interference of a donor in silicon, *Nature Materials* 13, 605–610 (2014) doi:10.1038/nmat3941
- [29] M. Usman, J. Bocquel, J. Salfi, B. Voisin, A. Tankasala, R. Rahman, M. Y. Simmons, S. Rogge and L. C. L. Hollenberg, Spatial metrology of dopants in silicon with exact lattice site precision, *Nature Nano*, (2016) DOI: 10.1038/NNANO.2016.83
- [30] V. Brazdova, DR.Bowler, K Sinthiptharakoon, P Studer, A Rahnejat, N J. Curson, S R. Schofield, and A J. Fisher, Exact location of dopants below the Si(001):H surface from scanning tunnelling microscopy and density functional theory, *Phys. Rev. B* 95, 075408 (2017)
- [31] A. Patané, N. Mori, O. Makarovskiy, L. Eaves, M. L. Zambrano, J. C. Arce, L. Dickinson, and D. K. Maude, "Manipulating and Imaging the Shape of an Electronic Wave Function by Magnetotunneling Spectroscopy" *Physical Review Letters* 105, 236804 (2010).
- [32] Wen Lei, Christian Notthoff, Jie Peng, Dirk Reuter, Andreas Wieck, Gabriel Bester, and Axel Lorke, "Artificial Atoms in Magnetic Fields: Wave-Function Shaping and Phase-Sensitive Tunneling" *Physical Review Letters* 105, 176804 (2010).

- [33] K. L. Litvinenko, M. Pang, Juerong Li, E. Bowyer, H. Engelkamp, V. B. Shuman, L. M. Portsel, A. N. Lodygin, Yu. A. Astrov, S. G. Pavlov, H.-W. Hübbers, C. R. Pidgeon, and B. N. Murdin. High-field impurity magneto-optics of Si:Se. *Phys. Rev. B* 90, 115204 (8 Sep 2014) DOI: 10.1103/PhysRevB.90.115204
- [34] Litvinenko KL, Li J, Stavrias N, Meaney AJ, Christianen PCM, Engelkamp H, Homewood KP, Pidgeon CR, Murdin BN, The quadratic Zeeman effect used for state-radius determination in neutral donors and donor bound excitons in Si:P, *Semiconductor Science and Technology* 31, 045007 (Apr 2016). DOI: 10.1088/0268-1242/31/4/045007
- [35] B.N. Murdin, Juerong Li, M.L. Y. Pang, E.T. Bowyer, K.L. Litvinenko, S.K. Clowes, H. Engelkamp, C.R. Pidgeon, I. Galbraith, N.V. Abrosimov, H. Riemann, S.G. Pavlov, H.-W. Hübbers & P.G. Murdin, Si:P as a laboratory analogue for hydrogen on high magnetic field white dwarf stars, *Nature Communications* 4, 1469 (2013) DOI: 10.1038/ncomms2466
- [36] R. A. Lewis, A. Bruno-Alfonso, G. V. B. de Souza, R. E. M. Vickers, J. A. Colla & E. Constable, Spherical, cylindrical and tetrahedral symmetries; hydrogenic states at high magnetic field in Si:P, *Scientific Reports* 3, 3488 (2013), doi:10.1038/srep03488
- [37] T. G. Castner, *Phys. Rev. B* 79, 195207 (2009)
- [38] Yu A Astrov, et al. Gas-phase doping of silicon with sulfur. *Semicond. Sci. Technol.* (2011) v.26, 055021 (4pp); doi:10.1088/0268-1242/26/5/055021;
- [39] Yu.A. Astrov, et al.. Planar sulfur-doped silicon detectors for high-speed infrared thermography. *Infrared Physics & Technology* (2009) v. 52, 25–31; doi:10.1016/j.infrared.2008.10.001
- [40] Yu.A. Astrov, et al. Development of photodetectors for image converters: Doping of silicon with selenium from the gas phase. *Semiconductors* (2008) v. 42, 448-452; doi: 10.1134/S1063782608040131
- [41] Yu. A. Astrov, V. B. Shuman, L. M. Portsel, A. N. Lodygin, S. G. Pavlov, N. V. Abrosimov, V. N. Shastin, H.-W. Hübbers. Diffusion doping of silicon with magnesium. *Phys. Status Solidi A* 214, No. 7, 1700192 (2017) / DOI 10.1002/pssa.201700192
- [42] B. Pajot, F. Merlet, G. Taravella, Quadratic Zeeman Effect of Donor Lines in Silicon. II. Comparison with Experiment, *Can J Phys*, 50, 2186 (1972) doi: 10.1139/p72-289
- [43] M Diarra, Y-M Niquet, C Delerue, and G Allan, Ionization energy of donor and acceptor impurities in semiconductor nanowires: Importance of dielectric confinement, *Phys Rev B* 75, 045301 (2007) DOI: 10.1103/PhysRevB.75.045301
- [44] Y. M. Niquet, D. Rideau, C. Tavernier, H. Jaouen, and X. Blase, *Phys. Rev. B* 79, 245201 (2009)
- [45] J. Mansir, P. Conti, Z. Zeng, J. J. Pla, P. Bertet, M. W. Swift, C. G. Van de Walle, M. L. W. Thewalt, B. Sklenard, Y. M. Niquet, and J. J. L. Morton *Phys. Rev. Lett.* 120, 167701 (2018)
- [46] M. Steger, et al *Phys Rev B* 79, 205210 (2009)